

A Structured Family of Grassmannian Constellations via Geodesic Mapping for MIMO Noncoherent Communications

Álvaro Pendás-Recondo[✉] and Enrique Pendás-Recondo[✉]

Abstract—This work presents a novel structured family of Grassmannian constellations for multiple-input multiple-output (MIMO) noncoherent communications over Rayleigh block-fading channels, where neither the transmitter nor the receiver has channel state information (CSI). The proposed constellation design is built upon the geodesic curves of the Grassmann manifold, thereby exploiting its underlying geometric structure. The resulting solution is limited in spectral efficiency (with a maximum constellation size of $4M^2$ points, where M is the number of transmit antennas), targeting a rate in the range of 0.25–1 bps/Hz. However, all space-time matrices resulting from this design exhibit the remarkable property of having a single nonzero entry per row, meaning that only one transmit antenna is active per time slot. This property significantly reduces hardware complexity and implementation cost, while also lowering power consumption, as only a single power amplifier is required for transmission. Furthermore, within the constellation size limits, the proposed design achieves error performance comparable to state-of-the-art optimization-based unstructured designs, as validated through symbol error rate (SER) numerical results. It also enables simple yet effective bit labeling, confirmed by comparisons of bit error rate (BER) and SER, and reduces the computational complexity of the maximum-likelihood (ML) detector for Grassmannian constellations by a factor of M .

Index Terms—Multiple-input multiple-output (MIMO), noncoherent communications, Grassmannian constellations, geodesics, Grassmann manifold, Rayleigh block-fading.

I. INTRODUCTION

MULTIPLE-input multiple-output (MIMO) communications have had a profound impact on wireless communications in recent decades, thanks to their enhanced spectral efficiency compared to single-input single-output (SISO)

The work of Álvaro Pendás-Recondo was supported in part by Ministerio de Ciencia e Innovación and Agencia Estatal de Investigación (MICIN)/(AEI)/10.13039/501100011033 under projects PID2023-146246OBC32 (ANT4IT) and PID2024-160783OA-I00 (RARIN-6G), cofunded by European Social Fund Plus (ESF+); and in part by the Gobierno del Principado de Asturias under grants Asturias-Sekuens/FEDER IDE-2024-000693, and “Severo Ochoa” Program Grant PA-22-BP21-116. The work of Enrique Pendás-Recondo was supported in part by Ministerio de Ciencia e Innovación and Agencia Estatal de Investigación (MICIN)/(AEI)/10.13039/501100011033 under project PID2021-124157NB-I00, cofunded by “ERDF A way of making Europe”; and in part by Fundación Séneca-Agencia de Ciencia y Tecnología de la Región de Murcia, under project “Ayudas a los proyectos para el desarrollo de investigación científica y técnica por grupos competitivos (Comunidad Autónoma de la Región de Murcia)”, included in “Programa Regional de Fomento de la Investigación Científica y Técnica (Plan de Actuación 2022)”, REF. 21899/PI/22.

Álvaro Pendás-Recondo is with the Group of Signal Theory and Communications, Department of Electrical Engineering, Universidad de Oviedo, 33203, Gijón, Spain (e-mail: pendasalvaro@uniovi.es). Enrique Pendás-Recondo is with the Group of Algebra, Department of Mathematics, Universidad de Oviedo, Oviedo 33007, Spain (e-mail: pendasenrique@uniovi.es).

systems. This advantage has been extensively demonstrated not only mathematically, in terms of system capacity, but also in practice through their widespread deployment in modern wireless standards, albeit with associated challenges [1].

A. Motivation: Coherent versus Noncoherent Schemes and Unitary Space-Time Modulation

One of the most significant challenges of MIMO is acquiring accurate channel state information (CSI). Channel state information at the transmitter (CSIT) in MIMO or multiple-input single-output (MISO) systems enables the application of digital precoding to achieve enhanced signal-to-noise ratio (SNR), diversity gain, or, only in MIMO, multiplexing gain. Channel state information at the receiver (CSIR) is required in standard MIMO, MISO, single-input multiple-output (SIMO), and SISO systems to ensure correct symbol decoding. CSIR in multi-antenna systems is typically obtained from the observation of orthogonal pilot symbols sent periodically by the transmitter, whereas CSIT is acquired through feedback from the receiver.

Although accurate CSIR is generally feasible to obtain, its main drawback lies in the reduction of spectral efficiency caused by pilot symbol transmission. This limitation becomes pronounced when the number of antennas is large, even in slowly varying channels, or when the channel varies rapidly, even with relatively few antennas [2]. Regarding CSIT, its accurate acquisition is considerably more challenging, as it is affected by factors that do not compromise CSIR, including limited and quantized feedback and feedback delays that lead to outdated CSIT, among others [3], [4]. Moreover, the feedback channel always consumes additional power and spectral resources.

In this context, noncoherent schemes, where neither the transmitter nor the receiver has CSI, are particularly attractive for short-packet communications with low-latency requirements and high user mobility, where conventional channel estimation is costly or unreliable. While not adopted in current wireless standards, they represent a promising research direction with potential applications in paradigms such as ultra-reliable low-latency communications (URLLC), Internet of Things (IoT) networks with significant energy and bandwidth constraints, and massive MIMO systems operating in rapidly time-varying channels [5].

The problem of noncoherent MIMO was first considered in [6] under Rayleigh block-fading. In this model, the channel

entries are independent and identically distributed (i.i.d.) and remain constant during the transmission of several symbols before adopting an independent realization drawn from a normal distribution. In [7], [8], and [9], further studies on the capacity of this scenario were conducted. Remarkably, noncoherent MIMO systems can achieve a significant fraction of the coherent capacity gain at high SNR, and this fraction increases with the number of time symbols over which the channel remains constant [9]. Furthermore, the use of unitary space-time modulation is an optimal solution in this scenario, in the sense that it minimizes the union bound of error probability under the assumption of equal-energy signals [8]. Consequently, this approach to the problem has been extensively studied [7], [8], [9], [10]. Mathematically, unitary space-time modulation is based on transmitting space-time matrices that are Stiefel representatives of points in the complex Grassmann manifold [11], which is why this solution is commonly referred to as Grassmannian signaling.

B. Related Works: Constellation Designs

For noncoherent MIMO communications, the problem of designing a Grassmannian constellation consists of finding a set of matrices that minimizes symbol error probability (SEP), with energy and power normalization inherently guaranteed by the unitary space-time condition. For the asymptotic case with an infinite number of points, the optimal design approach is to randomly sample the Grassmann manifold. However, in practical scenarios with a finite number of constellation points, the problem becomes considerably more complex. The packing problem on the Grassmann manifold endowed with a Riemannian metric—which induces the natural notion of distance on the manifold, also known as geodesic distance—remains unsolved for an arbitrary number of points [12]. Furthermore, beyond the geodesic distance, other figures of merit have been investigated for minimizing SEP or pairwise error probability (PEP), which, depending on the scenario, may serve as more effective predictors. Examples include the chordal distance [13], [14], the diversity product (DP) [15], [16], also known as the coherence criterion, and the asymptotic union bound (UB) [17], [18].

In general, constellation designs in the literature can be classified into two categories: structured and unstructured [5], [18]. The first category imposes a certain structure on the space-time matrices, which simplifies both the design process and symbol decoding [19], [20], [21], [22], [23]. This is a considerable advantage, since the computational complexity of the maximum-likelihood (ML) detector for arbitrary Grassmannian constellations represents a major challenge for practical implementation as the number of points (and thus the spectral efficiency) increases. On the other hand, unstructured designs do not impose any specific restrictions and rely on numerical optimization, typically with the primary goal of improving error probability performance [18], [24], [25], [26], in which they generally surpass structured designs. However, they have the disadvantage of yielding non-deterministic solutions, and the absence of structure makes it difficult to reduce the computational complexity of ML detection. To the best of our

knowledge, the work in [18], based on gradient optimization of the UB criterion, provides the best unstructured Grassmannian constellation designs in terms of reported numerical SER results, followed closely by the earlier work in [26], which was based on gradient optimization of the DP (coherence criterion).

Related to this problem, the noncoherent SIMO scenario (which can be considered a particular instance of the MIMO case) has recently garnered considerable attention [27], [28], [29], [30]. In this context, unitary (or Grassmannian) signaling has also been shown to be an effective solution in practical scenarios [27], [28]. The inherent simplicity of the SIMO case compared to MIMO enables low-complexity designs that are particularly appealing for uplink communications. Finally, a promising yet largely unexplored research direction is the design of Grassmannian constellations for noncoherent multi-user MIMO, a field where some recent works have already contributed [31].

C. Contributions

The main contributions of this work are summarized as follows:

- We present a novel family of structured Grassmannian constellations. The proposed solution is built upon the geodesic curves of the Grassmann manifold, thereby exploiting its underlying geometric structure. The design consists of computing geodesics on the Grassmann manifold from a chosen initial point, along with an appropriate set of initial velocities. These geodesics are then mapped to extract constellation points with desirable properties for error performance.
- The proposed family is limited in spectral efficiency (with a maximum constellation size of $4M^2$ points, where M is the number of transmit antennas), but offers one significant advantage that, to the best of our knowledge, is not present in any previous Grassmannian signaling design: all resulting space-time matrices have a single nonzero element per row, i.e., only one active antenna is required per time slot. This has important implications for practical implementation: at the transmitter, only one digital-to-analog (DAC) chain is required, together with a switch to select the corresponding antenna at each time slot. This not only simplifies the hardware but also reduces power consumption, as only a single active power amplifier is required for transmission.
- Antenna selection in MIMO is a well-known solution in the literature [32], typically offering a tradeoff between reduced hardware complexity and cost on the one hand, and system performance on the other. However, the proposed structured family of Grassmannian constellations achieves comparable symbol error rate (SER) performance to state-of-the-art optimization-based unstructured designs, as validated through numerical simulations.
- Additionally, the proposed design reduces the computational complexity of the ML detector by a factor of M and also simplifies bit labeling. To validate the latter point, comparisons between SER and bit error rate (BER) are presented.

- Although we again remark that our solution is limited in spectral efficiency, the considered range of constellation points is arguably one of the most interesting for the application of noncoherent MIMO, since larger constellations are subject to a high computational detection cost, especially in unstructured designs aimed at optimizing error performance. In this sense, the presented approach offers relatively low spectral efficiencies (0.25–1 bps/Hz) but achieves error performance comparable to state-of-the-art solutions for noncoherent MIMO within this range, while enabling low-cost and low-complexity hardware implementation. In fact, the proposed design may find applicability in scenarios where SIMO has previously been considered, offering enhanced error performance by simply adding a switching scheme and multiple antennas at the transmitter, without the need for additional DAC chains or power amplifiers.

The remainder of this paper is organized as follows. Section II introduces the system model for noncoherent MIMO communications with Grassmannian signaling. Section III reviews the metrics related to the Grassmann manifold that can predict PEP and SEP and thus guide the design of constellations. Section IV describes the proposed constellation design, while Section V provides numerical results based on Monte Carlo simulations for SER and BER. Finally, conclusions are drawn in Section VI. In addition, Appendix-A provides the theoretical background on the Grassmann and Stiefel manifolds required for this work, along with mathematical proofs of the proposed theorems.

Notation: Scalars are denoted by italic letters (either lowercase or uppercase, x , X), while matrices are denoted by bold uppercase letters, \mathbf{X} . Subspaces and sets are denoted by calligraphic letters, \mathcal{X} . The transpose, conjugate transpose, determinant, and trace of a matrix are denoted by $(\cdot)^T$, $(\cdot)^H$, $\det(\cdot)$, and $\text{tr}(\cdot)$, respectively. The identity matrix of size M is written as \mathbf{I}_M , and $\mathbf{0}_M$ denotes a square matrix of size M with all entries equal to zero. The real and imaginary parts of a scalar or matrix are denoted by $\Re(\cdot)$ and $\Im(\cdot)$, respectively. The absolute value of a scalar, or the cardinality of a set, is denoted by $|\cdot|$, and the floor of a scalar, as $\lfloor X \rfloor$. $E\{\cdot\}$ is the expected value. The Frobenius norm of a matrix is written as $\|\mathbf{X}\|_F$. A complex Gaussian distribution with mean μ and variance σ^2 is denoted by $\mathcal{CN}(\mu, \sigma^2)$. Appendix-A provides the necessary theoretical background on the Grassmann and Stiefel manifolds, along with their more specific notation.

II. SYSTEM MODEL

A. System Model

Consider a MIMO wireless system where a transmitter equipped with M antennas communicates with a receiver with N antennas over a frequency-flat block-fading channel with a coherence of T symbols, $T \geq 2M$. Consequently, it is assumed that the channel matrix $\mathbf{H} \in \mathbb{C}^{T \times N}$ remains constant during each block of T symbols, and changes to an independent realization in the next block. The channel entries, $h_{ij} \in \mathbb{C}$, are i.i.d. and follow a normal distribution with zero mean and unit variance, i.e., $h_{ij} \sim \mathcal{CN}(0, 1)$,

according to classical Rayleigh fading. Furthermore, the channel realizations are unknown to both the transmitter and the receiver, a scenario commonly referred to as a noncoherent communication.

Within a block of T symbols, the transmitter sends a matrix $\mathbf{X} \in \mathbb{C}^{T \times M}$, such that $\mathbf{X}^H \mathbf{X} = \mathbf{I}_M$. The matrix \mathbf{X} is a Stiefel representative of a point $[\mathbf{X}]$ in the complex Grassmann manifold $\text{Gr}_{\mathbb{C}}(T, M)$, as described in Appendix-A. For each time block, the transmit matrix is chosen uniformly from an alphabet $\mathcal{X} = \{\mathbf{X}_1, \mathbf{X}_2, \dots, \mathbf{X}_L\}$, so $|\mathcal{X}| = L$. The alphabet \mathcal{X} is also denoted as the codebook or the constellation for the communication, and its elements, as the constellation points. For a given constellation, the rate of the communication is determined by $R = \log_2(L)/T$ (bps/Hz) and each codeword carries $\log_2(L)$ bits of information.

The signal at the receiver over a time block is denoted as $\mathbf{Y} \in \mathbb{C}^{T \times N}$ and it is given by

$$\mathbf{Y} = \mathbf{X}\mathbf{H} + \sqrt{\frac{M}{T\rho}}\mathbf{W}, \quad (1)$$

where $\mathbf{W} \in \mathbb{C}^{T \times N}$ represents the additive white Gaussian noise (AWGN), i.e., its entries are i.i.d. with $w_{ij} \sim \mathcal{CN}(0, 1)$ and ρ denotes the signal-to-noise ratio (SNR). Assuming Rayleigh block-fading, the optimal ML detector that minimizes error probability is [7]

$$\hat{\mathbf{X}} = \arg \max_{\mathbf{X} \in \mathcal{X}} \text{tr}(\mathbf{Y}^H \mathbf{P}_{[\mathbf{X}]} \mathbf{Y}), \quad (2)$$

where $\mathbf{P}_{[\mathbf{X}]} = \mathbf{X}\mathbf{X}^H$ is the projector onto the subspace $\text{span}(\mathbf{X})$ (see Appendix-A).

B. Grassmannian Signaling Application

The capacity of the noncoherent block-fading channel model under consideration was first studied in [6]. Unitary space-time modulation was proposed in [7] as a solution to the problem and demonstrated optimal in [8] in the sense that it minimizes the union bound of error probability under the assumption of equal-energy signals. In this context, note that Grassmannian signaling and unitary space-time modulation refer to the same concept, that is, $\mathbf{X}\mathbf{X}^H = \mathbf{I}_M$, which is equivalent to stating that the columns of \mathbf{X} are orthonormal. In [9], it was shown that, at high SNR, the degrees of freedom of the system are $M^* \left(1 - \frac{M^*}{T}\right)$, where $M^* = \min\{M, N, \lfloor T/2 \rfloor\}$, and that the use of Grassmannian signaling is optimal for ergodic capacity when $T \geq \min\{M, N\} + N$. Furthermore, for a given T , the optimal number of transmit antennas is $\lfloor T/2 \rfloor$ (as additional transmit antennas do not increase capacity), while the number of receive antennas should be no less than $\lfloor T/2 \rfloor$. Along the same lines, the numerical mutual information results presented in [10] also concluded that, at high SNR, mutual information is maximized when $M = \min\{N, \lfloor T/2 \rfloor\}$.

In the case $T < M + N$, Grassmannian signaling is no longer optimal [33], since it does not achieve capacity at high SNR. The corresponding capacity-achieving input signal, introduced in [33], is referred to as beta-variate space-time

modulation and does not satisfy the equal-energy condition, as different transmitted matrices may have different energy levels. Nevertheless, for beta-variate space-time modulation, numerical results also indicate that the optimal number of transmit antennas is $M = \lfloor T/2 \rfloor$, while the rate gain becomes significant compared to Grassmannian signaling only when $N \gg T$.

The structured family of Grassmannian constellations presented in this paper is designed for any number of transmit antennas $M = 1, 2, 3, 4, \dots$, with $T = 2M$, and for any number of receive antennas. Based on previous results, the most suitable application scenario is when $T = M + N = 2M$, i.e., $N = M$ and $M = T/2$, in which case Grassmannian signaling is the optimal choice for noncoherent communication in the Rayleigh block-fading channel. Nonetheless, in Section V SER and BER results are presented for different numbers of receive antennas for a given M , while maintaining $T = 2M$, in order to illustrate error performance differences consistent with the mutual information results reported in the literature.

Note that the condition $T = 2M$ can always be imposed by the system. For instance, if in a practical implementation the channel remains quasi-constant during an odd number of symbols, e.g., $T = 7$, the system can transmit using a coherence block of $T = 6$ with $M = 3$ transmit antennas. Another option would be to use the full coherence block with $T = 7$, setting $M = \lfloor T/2 \rfloor = 3$ and $N = 4$, so that $M + N = T$, in which case Grassmannian signaling remains optimal. However, the increase in the degrees of freedom of the system is rather limited, according to the previously presented expression $M^* \left(1 - \frac{M^*}{T}\right)$ with $M^* = \min\{M, N, \lfloor T/2 \rfloor\}$, [9]. Furthermore, the applicability of the scheme (even T and even M greater than 1 but different from N) would be limited.

III. METRICS AND ERROR PROBABILITY

The relationship between various metrics related to the Grassmann manifold and the error probability of a given constellation in the block-fading channel described in Section II has been extensively studied in the literature [13], [15], [16], [17], [18], [26]. Most of these metrics are related to the principal angles between two points on the Grassmann manifold, defined in Eq. (13). The principal angles also determine the geodesic distance between two points, d_g , given in Eq. (14), which is the natural notion of Riemannian distance, as explained in Appendix-A. Note that, strictly speaking, points in the Grassmannian are subspaces and should be denoted as $[\mathbf{X}]$. However, when computing distances or metrics between two constellation points, we omit brackets for simplicity and write \mathbf{X} .

One of the most widely used metrics for designing Grassmannian constellations for noncoherent communications is the chordal distance [13], [14], which we denote by d_c and which is defined as

$$\begin{aligned} d_c(\mathbf{X}_i, \mathbf{X}_j) &= \frac{1}{\sqrt{2}} \|\mathbf{P}_{[\mathbf{x}_i]} - \mathbf{P}_{[\mathbf{x}_j]}\|_F \\ &= \left(\sum_{m=1}^M \sin^2 \theta_m \right)^{1/2}, \end{aligned} \quad (3)$$

where, based on the definition of the principal angles, θ_m , it is clear that the maximum value for the chordal distance is \sqrt{M} .

However, the study presented in [16] revealed that the chordal distance between two constellation points is related to their PEP only at low SNR, while at high SNR, the so-called DP is a better criterion for minimizing the PEP between two codewords. The DP between two constellation points is defined as [15], [16]

$$\begin{aligned} \text{DP}(\mathbf{X}_i, \mathbf{X}_j) &= \det(\mathbf{I}_M - \mathbf{X}_i^H \mathbf{X}_j \mathbf{X}_j^H \mathbf{X}_i) \\ &= \prod_{m=1}^M \sin^2 \theta_m. \end{aligned} \quad (4)$$

In general, when designing a constellation based on either the chordal distance or DP, the goal is to maximize the minimum value across all possible pairs. In this context, it is useful to define the chordal distance of a constellation \mathcal{X} as

$$d_c(\mathcal{X}) = \min_{i \neq j} d_c(\mathbf{X}_i, \mathbf{X}_j), \quad (5)$$

and the DP of a constellation as

$$\text{DP}(\mathcal{X}) = \min_{i \neq j} \text{DP}(\mathbf{X}_i, \mathbf{X}_j), \quad (6)$$

where the objective of minimizing $\text{DP}(\mathcal{X})$ is also known as the coherence criterion [26].

Based on the previous explanation, note that the chordal and DP approaches focus on improving the worst-case PEP. This strategy is standard for Gaussian channels affected only by AWGN, where the SEP is typically dominated by the largest PEP. However, under Rayleigh fading, particularly at medium or low SNR, considering codeword pairs beyond the worst case may significantly improve the accuracy of SEP approximations. In [17] and [18], the asymptotic UB is presented as a metric that accounts for all codeword pairs when evaluating a constellation. In [18], the UB at high SNR is defined, up to a constant, as

$$\text{UB}(\mathcal{X}) = \sum_{i < j} \det(\mathbf{I}_M - \mathbf{X}_i^H \mathbf{X}_j \mathbf{X}_j^H \mathbf{X}_i)^{-N}, \quad (7)$$

where, remarkably, the number of receive antennas, N , appears explicitly in the expression. In this case, minimizing the UB of the constellation is desirable, as it has been proven in [18] and [34] to be a tight bound on the PEP as $\rho \rightarrow \infty$.

In [18], a gradient descent optimization is presented to minimize the UB for arbitrary values of (T, M, N, L) . To the best of our knowledge, the work in [18] provides the best Grassmannian constellation designs in terms of reported numerical SER results. Finally, Table III summarizes the considered metrics.

IV. CONSTELLATION DESIGN

In this section, we present the algorithm for designing Grassmannian constellations using geodesic mapping. The input parameters are the number of transmit antennas, M (with $T = 2M$, as described in Section II-B), and the number of

TABLE I
METRICS AND RELATIONSHIP TO PEP.

Metric	Definition	Range	Goal	PEP relationship
Geodesic distance	$d_g(\mathbf{X}_i, \mathbf{X}_j) = \left(\sum_{m=1}^M \theta_m^2 \right)^{1/2}$ $d_g(\mathcal{X}) = \min_{i \neq j} d_g(\mathbf{X}_i, \mathbf{X}_j)$	$[0, \sqrt{M} \frac{\pi}{2}]$	-	-
Chordal distance	$d_c(\mathbf{X}_i, \mathbf{X}_j) = \left(\sum_{m=1}^M \sin^2 \theta_m \right)^{1/2}$ $d_c(\mathcal{X}) = \min_{i \neq j} d_c(\mathbf{X}_i, \mathbf{X}_j)$	$[0, \sqrt{M}]$	Max. min.	Worst pair, low SNR
Diversity product (DP)	$DP(\mathbf{X}_i, \mathbf{X}_j) = \prod_{m=1}^M \sin^2 \theta_m$ $DP(\mathcal{X}) = \min_{i \neq j} DP(\mathbf{X}_i, \mathbf{X}_j)$	$[0, 1]$	Max. min.	Worst pair, high SNR
Union bound (UB)	$UB(\mathcal{X}) = \sum_{i < j} \det \left(\mathbf{I}_M - \mathbf{X}_i^H \mathbf{X}_j \mathbf{X}_j^H \mathbf{X}_i \right)^{-N}$	$[1, \infty)$	Minimize	All pairs, high SNR

constellation points, L , where L is a power of two that satisfies $2 \leq L \leq 4M^2$. The goal is to obtain a constellation \mathcal{X} with two properties: first, all constellation points must satisfy that each row of the transmitted space-time matrix contains a single nonzero entry, i.e., only one antenna is active per time slot; second, error performance at least comparable to previous constellation designs, as validated in Section V-C. Additionally, the algorithm inherently simplifies the problem of bit labeling, as explained in Section IV-C, and the second property reduces the computational complexity of the ML detector, as detailed in Section IV-D.

As stated in Section I-C, the spectral efficiency is limited by the maximum number of points, $4M^2$, as shown in Table II, since $R = \log_2(L)/T$ (see Section II). However, it should be noted that higher spectral efficiency values with arbitrary Grassmannian constellations are constrained by the computational cost at the receiver when ML detection is applied. As explained in Section IV-D, the computational cost of the ML detector for arbitrary Grassmannian constellations is $\mathcal{O}(LMTN)$, which quickly becomes dominated by L as spectral efficiency increases. For example, consider the case $T = 8$ and $M = 4$ with a spectral efficiency of 1.5 bps/Hz. This requires $L = 4096$ points, exceeding the maximum considered even for unstructured designs (e.g., up to $L = 2048$ points in [18]). This further reinforces the fact that rates in the range of 0.25–1 bps/Hz are particularly relevant for the application of Grassmannian signaling in MIMO noncoherent schemes. Although designs with significantly higher spectral efficiency have been proposed, particularly for the SIMO case [27], they achieve this at the expense of reduced error performance, as ML detection is not applied.

A. Geodesics and Diametral Sets

We now present the mathematical results and the specific choices on which our design is based. We refer the reader to Appendix-A for the definitions of the mathematical objects and notions used here.

Theorem 1. Let $[\mathbf{U}] \in \text{Gr}_{\mathbb{C}}(2M, M)$ be a point and $\Delta \in$

TABLE II
MAXIMUM NUMBER OF POINTS AND SPECTRAL EFFICIENCY.

(T, M)	Maximum number of points	Maximum spectral efficiency
(2, 1)	4	1 bps/Hz
(4, 2)	16	1 bps/Hz
(6, 3)	36 (32)	5/6 bps/Hz
(8, 4)	64	0.75 bps/Hz
(16, 8)	256	0.5 bps/Hz

$T_{[\mathbf{U}]} \text{Gr}_{\mathbb{C}}(2M, M)$ a vector of the form

$$\mathbf{U} = \begin{pmatrix} \tilde{\mathbf{U}} \\ \mathbf{0}_M \end{pmatrix}, \quad \Delta = \begin{pmatrix} \mathbf{0}_M \\ \tilde{\Delta} \end{pmatrix}, \quad (8)$$

where $\tilde{\mathbf{U}} \in \text{St}_{\mathbb{C}}(M, M)$ and $\tilde{\Delta} \in \mathbb{C}^{M \times M}$. If $\sqrt{M} \tilde{\Delta} \in U(M)$, then Δ is a diametral vector and the geodesic γ_{Δ} admits the following expression:

$$\gamma_{\Delta}(t) = \left[\begin{pmatrix} \cos \left(\frac{t}{\sqrt{M}} \right) \tilde{\mathbf{U}} \\ \sqrt{M} \sin \left(\frac{t}{\sqrt{M}} \right) \tilde{\Delta} \end{pmatrix} \right], \quad \forall t \in \mathbb{R}. \quad (9)$$

Proof. See Appendix-B. \square

The key implication of this result is that, if we choose $\tilde{\mathbf{U}}$ and $\tilde{\Delta}$ so that each row contains only one nonzero entry, then each geodesic point admits a Stiefel representative that inherits this property. Our proposal is therefore to obtain the constellation points from Eq. (9) by carefully selecting one point \mathbf{U} and $4M^2$ vectors Δ in the form of Eq. (8).

To select suitable vectors, we first remark that, for any \mathbf{U} in the form of Eq. (8), it is always possible to construct a basis $\{\Delta_k\}_{k=1}^{2M^2}$ of $T_{[\mathbf{U}]} \text{Gr}_{\mathbb{C}}(2M, M)$ satisfying the following properties:

- Each Δ_k has the form of Eq. (8) and $\sqrt{M} \tilde{\Delta}_k \in U(M)$, i.e., $\Delta_k^H \Delta_k = \tilde{\Delta}_k^H \tilde{\Delta}_k = \frac{1}{M} \mathbf{I}_M = \tilde{\Delta} \tilde{\Delta}^H$. In particular, this implies that every Δ_k is g -unit (with respect to the Riemannian metric g in Eq. (12)).

- $\{\Delta_k\}_{k=1}^{2M^2}$ is g -orthonormal, i.e., $g_{[\mathbf{U}]}(\Delta_k, \Delta_l) = \delta_{kl}$, where δ_{kl} is the Kronecker delta.
- Each Δ_k has only one nonzero entry in each row.

The first condition ensures that every vector of the basis satisfies the hypotheses of Theorem 1. The second condition, together with the fact that each Δ_k is diametral (by Theorem 1), allows us to fully exploit the distribution of the geodesics over the manifold. The last condition, if also satisfied by $\tilde{\mathbf{U}}$, guarantees that the constellation points obtained from Eq. (9) have exactly one nonzero entry per row. One example of such a basis is given by the g -normalized Weyl-Heisenberg matrices (the canonical matrix representation of the finite-dimensional Weyl-Heisenberg group; see, for example, [35, Chapter 12] and [36]). Finally, observe that given $\{\Delta_k\}_{k=1}^{2M^2}$, their opposites $\{-\Delta_k\}_{k=1}^{2M^2}$ also form a basis of $T_{[\mathbf{U}]} \text{Gr}_{\mathbb{C}}(2M, M)$ with the same properties.

Taking all this into account, we make the following explicit choices for \mathbf{U} and Δ of the form of Eq. (8): since there are no privileged points in the Grassmannian, we set $\tilde{\mathbf{U}} = \mathbf{I}_M$ for simplicity, and we select the $4M^2$ vectors $\{\pm\Delta_k\}_{k=1}^{2M^2}$, where each Δ_k is a g -normalized Weyl-Heisenberg matrix. In the constellation design, each vector provides a single constellation point by choosing a suitable $t \in \mathbb{R}$ in Eq. (9), yielding a maximum of $4M^2$ constellation points.

For the DP and UB metrics (Section III), we are interested in constellation points whose pairwise principal angles are all nonzero. At the same time, we must also ensure good performance with respect to the geodesic and chordal distances by distributing the constellation points as far apart as possible over the manifold. To identify such points, we make use of the following results.

Theorem 2. Within the hypotheses of Theorem 1, let $\gamma_{\Delta_1}(t_1)$ and $\gamma_{\Delta_2}(t_2)$ be two geodesic points satisfying Eq. (9), with $t_1, t_2 \in (0, \sqrt{M}\frac{\pi}{2})$. Then:

- If $t_1 \neq t_2$, all the principal angles between both geodesic points are nonzero.
- If $t_1 = t_2$, the number of principal angles equal to zero between both geodesic points coincides with the number of eigenvalues of $M\Delta_1^H\Delta_2$ equal to 1.

Proof. See Appendix-C. \square

Corollary 1. Let $\Delta \in T_{[\mathbf{U}]} \text{Gr}_{\mathbb{C}}(2M, M)$ be a vector satisfying the hypotheses of Theorem 1. Then, all the principal angles between $\gamma_{\Delta}(\sqrt{M}\frac{\pi}{4})$ and $\gamma_{-\Delta}(\sqrt{M}\frac{\pi}{4})$ are equal to $\frac{\pi}{2}$.

Proof. See Appendix-D. \square

This means that geodesic points associated with opposite vectors, when taken halfway along the geodesic, exhibit exactly the properties we are looking for: all their principal angles are maximal (in particular, nonzero), which in turn implies that they are separated by the maximum possible geodesic and chordal distances in the Grassmann manifold. Therefore, in our design, we are interested in obtaining constellation points from vector pairs $\pm\Delta$ whenever possible, while ensuring at the same time that constellation points coming from different pairs do not have any principal angle equal to zero. With this

in mind, we say that $\mathcal{G} \subset \{\pm\Delta_k\}_{k=1}^{2M^2}$ is a *diametral set* if it satisfies the following conditions:

- For any two vectors $\Delta_1, \Delta_2 \in \mathcal{G}$, there is no eigenvalue of $M\Delta_1^H\Delta_2$ equal to 1.
- If $\Delta \in \mathcal{G}$, then $-\Delta \in \mathcal{G}$.

By Theorem 2, the first condition means that all the principal angles between $\gamma_{\Delta_1}(t)$ and $\gamma_{\Delta_2}(t)$ are nonzero for all $t \in (0, \sqrt{M}\frac{\pi}{2})$. The second condition guarantees that, within the same diametral set \mathcal{G} , we can exploit the properties of geodesic points associated with opposite vectors $\pm\Delta \in \mathcal{G}$. Note that both conditions are consistent, thanks to Corollary 1; in fact, all the eigenvalues of $-M\Delta_k^H\Delta_k = -\mathbf{I}_m$ are equal to -1 . Given M , we denote by D the size of the largest diametral set that can be constructed from $\{\pm\Delta_k\}_{k=1}^{2M^2}$.

B. Algorithm Description

Given the background developed in Section IV-A, we now present our proposed constellation design algorithm, Algorithm 1. Note that the maximum size of a diametral set, D , is deterministic and determined by M (which defines $\text{Gr}_{\mathbb{C}}(2M, M)$) and the chosen vector basis, and it can be readily obtained numerically by testing vector combinations. As an illustrative example of the algorithm, consider the case $M = 2$ (thus $T = 4$), which yields $D = 8$. Table III presents the obtained results for all possible values of L in terms of $d_g(\mathcal{X})$, $d_c(\mathcal{X})$, and $DP(\mathcal{X})$.

Algorithm 1 Constellation Design

Input: M (which defines T and D), and L , $2 \leq L \leq 4M^2$

Output: Constellation \mathcal{X} , $|\mathcal{X}| = L$

- 1: **if** $L = 2$ **then**
- 2: {Case (i)}
- 3: Select one Δ_k and take the two points $\gamma_{\Delta_k}(0)$ and $\gamma_{\Delta_k}(\sqrt{M}\frac{\pi}{2})$
- 4: **else if** $L = 4$ and $D \geq 4$ **then**
- 5: {Case (ii)}
- 6: Select two vector pairs in the same diametral set \mathcal{G} , $\pm\Delta_1$ and $\pm\Delta_2$, and adjust geodesic mapping taking the four points $\gamma_{\pm\Delta_1}(\sqrt{M}\frac{\pi}{4} + x)$, $\gamma_{\pm\Delta_2}(\sqrt{M}\frac{\pi}{4} - x)$
- 7: **else if** $2 < L \leq D$ **then**
- 8: {Case (iii)}
- 9: Select any diametral set \mathcal{G} of size L , and take the points $\gamma_{\pm\Delta_k}(\sqrt{M}\frac{\pi}{4})$
- 10: **else if** $D < L \leq 2D$ **then**
- 11: {Case (iv)}
- 12: Select any two diametral sets \mathcal{G}_1 and \mathcal{G}_2 of size $L/2$ without any repeated vectors, $\mathcal{G}_1 \cap \mathcal{G}_2 = \emptyset$, and adjust geodesic mapping taking the points $\gamma_{\Delta_1}(\sqrt{M}\frac{\pi}{4} + x)$ for all $\Delta_1 \in \mathcal{G}_1$, and $\gamma_{\Delta_2}(\sqrt{M}\frac{\pi}{4} - x)$ for all $\Delta_2 \in \mathcal{G}_2$
- 13: **else**
- 14: {Case (v)}
- 15: Take the points $\gamma_{\pm\Delta_k}(\sqrt{M}\frac{\pi}{4})$ for any $L/2$ vector pairs $\pm\Delta_k$
- 16: **end if**

TABLE III
ALGORITHM PERFORMANCE FOR $T = 4, M = 2$

L	$d_g(\mathcal{X})$	$d_c(\mathcal{X})$	$DP(\mathcal{X})$
2	$\sqrt{2}\frac{\pi}{2}$	$\sqrt{2}$	1
4	1.3508	1.1546	0.4442
8	1.1107	1	0.25
16	0.9888	0.9102	0.1715

For Case (i) in Algorithm 1, the solution is optimal with respect to all metrics in Table III, since all principal angles between the two points are equal to $\frac{\pi}{2}$. For Case (iii), the diametral set ensures that no zero principal angles exist between points in the constellation, and, additionally, mapping all geodesics at their midpoint provides good performance in terms of chordal distance. In Case (ii) and Case (iv), the geodesic mapping is adjusted through a single parameter, x . For Case (ii), compared to Case (iii), having only two vector pairs allows an adjustment that can be used to further enhance performance. In Case (iv), this adjustment becomes necessary to ensure a nonzero DP, since two diametral sets are involved. Both cases are illustrated in Fig. 1 for $T = 4, M = 2$, where the dotted line indicates the value of x that minimizes the UB when $N = 2$. Remarkably, in Fig. 1a (Case (ii)), the optimal mapping point is the same across all metrics. In contrast, in Fig. 1b, choosing the value of x that maximizes DP slightly reduces the chordal and geodesic distances, though this value remains close to the one that minimizes UB. In general, for Case (ii) and Case (iv) with any T and M , we select the value of x that maximizes DP. In all observed scenarios, this x is close to the value that minimizes UB (although this value varies slightly with N). As a result, choosing DP instead of UB has only a minor impact on the resulting constellation points and, consequently, a negligible effect on error performance (see Section V-B), while it is worth noting that the proposed algorithm supports both options.

Finally, for Case (v), numerical results obtained by adjusting geodesic mapping for more than two sets achieve poor performance compared to gradient-based optimization approaches in terms of either UB [18] or DP [26]. Consequently, we forgo DP or UB optimization and instead adopt an approach focused on chordal distance. Remarkably, when mapping all $L = 4M^2$ geodesics using the Weyl–Heisenberg matrices (Section IV-A) at $\sqrt{M}\frac{\pi}{4}$, the minimum chordal distance between points is $\sqrt{M}/\sqrt{2}$, i.e., the maximum possible chordal distance in the Grassmann manifold scaled by $1/\sqrt{2}$. Although not mathematically proven here, this result has been validated numerically for $M = 1, 2, \dots, 8$ and demonstrates excellent chordal distance performance for $L = 4M^2$ points, leading to strong error performance at low SNR (see Section V-C).

C. Bit Labeling

Once a constellation with the target number of points L is obtained according to Algorithm 1, the proposed bit labeling assigns pairs of codewords with the largest Hamming distance to points mapped on geodesics departing in opposite directions

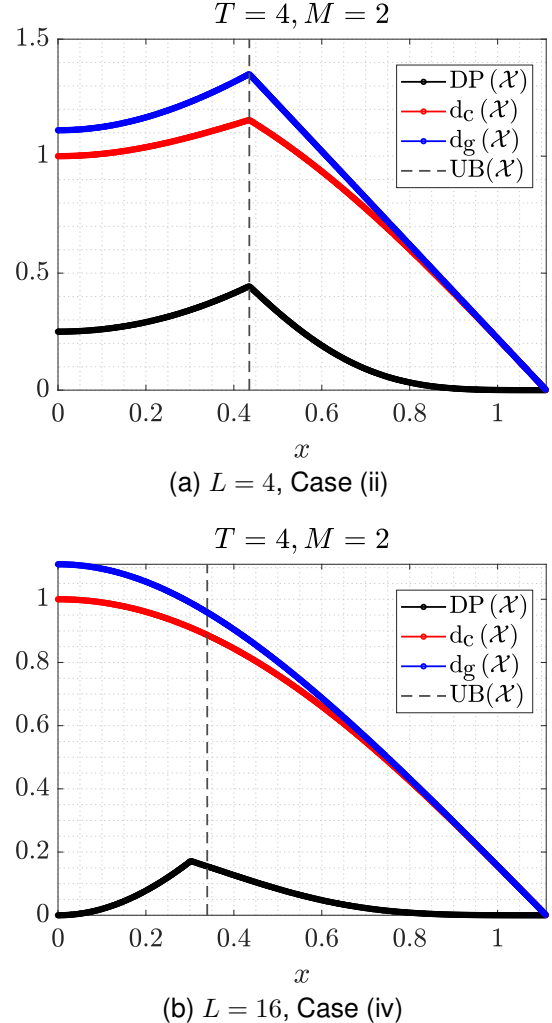


Fig. 1. Constellation metrics versus geodesic mapping parameter, x , for Case (ii) and Case (iv) of Algorithm 1 with $T = 4$ and $M = 2$. For the UB, the dotted line indicates the value of x that achieves its minimum when $N = 2$. A total of 5000 values of x are shown.

($\pm\Delta_k$). Note that this is always feasible, since vectors are selected in pairs for any even L . This guarantees that all principal angles between points with maximum Hamming distance are maximal within the constellation (and always nonzero, Section IV-A) and that such pairs achieve the lowest PEP.

D. Receiver Computational Complexity

Assuming the use of the ML detector, the argument in Eq. (2) can be rewritten as

$$\begin{aligned} \text{tr}(\mathbf{Y}^H \mathbf{P}_{[\mathbf{X}]} \mathbf{Y}) &= \text{tr}(\mathbf{Y}^H \mathbf{X} \mathbf{X}^H \mathbf{Y}) \\ &= \text{tr}((\mathbf{X}^H \mathbf{Y})^H (\mathbf{X}^H \mathbf{Y})) = \|\mathbf{X}^H \mathbf{Y}\|_F^2, \end{aligned} \quad (10)$$

where the computational complexity of evaluating this argument is dominated by the matrix multiplication $\mathbf{X}^H \mathbf{Y}$, which, for arbitrary Grassmannian constellations, results in a total complexity of $\mathcal{O}(LMTN)$ when comparing the L possible codewords. However, for the proposed family of constellations, since each row of \mathbf{X} contains a single nonzero entry

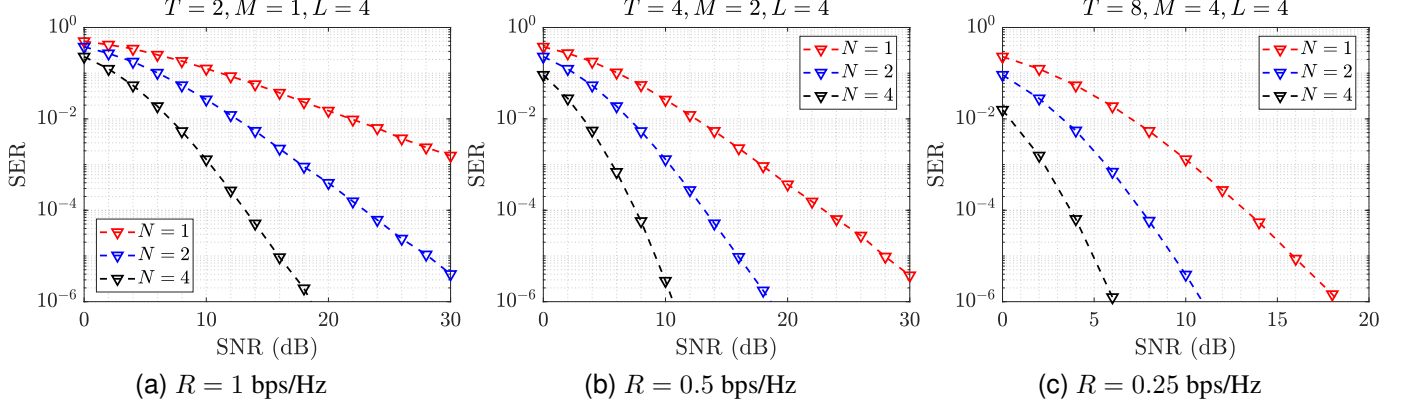


Fig. 2. SER results for $L = 4$ constellation points and different values of T , M , and N .

whose position is known to the receiver, the multiplication $\mathbf{X}^H \mathbf{Y}$ can be performed by simply adding scaled rows of \mathbf{Y} . This reduces the complexity to $\mathcal{O}(LTN)$, yielding an improvement by a factor of M .

V. NUMERICAL RESULTS

In this section, we present numerical results based on SER and BER Monte Carlo simulations to evaluate the error performance of the designed constellations. In all cases, we consider the block-fading channel presented in Section II and the ML detector described in Eq. (2). For this scenario, the SNR is defined in Eq. (1) by the term ρ . We always consider $T = 2M$ (Section II-B), and $2 \leq L \leq 4M^2$, being L a power of two and its maximum restricted by the proposed constellation design (Section IV).

A. SER Performance

We begin by analyzing the SER performance of the proposed family of Grassmannian constellations across different scenarios. Fig. 2 presents the SER results for a small constellation size, $L = 4$, under different values of T , M , and N . For the considered cases $T = 2$, $T = 4$, and $T = 8$, the corresponding spectral efficiencies are $R = 1$, $R = 0.5$, and $R = 0.25$ bps/Hz, respectively. As expected, for a fixed number of constellation points, increasing the dimensions determined by (T, M) consistently improves the SER performance for the same value of receive antennas, N . Furthermore, for each pair (T, M) , and consistent with previous theoretical results in the literature (Section II-B), the number of receive antennas should be at least $N = \lfloor T/2 \rfloor$ [9]. This behavior is confirmed in Fig. 2b and Fig. 2c, where a remarkable improvement in performance is observed when N reaches $N = 2$ and $N = 4$, respectively. Nevertheless, as observed across all figures, increasing the number of receive antennas continues to have a remarkable impact on SER performance, even when $N > \lfloor T/2 \rfloor$. Although, as explained in Section II-B, when $T < M + N$ the capacity of Grassmannian signaling is outperformed by beta-variance space modulation, this difference becomes significant only when $N \gg T$ [33]. This justifies studying the application

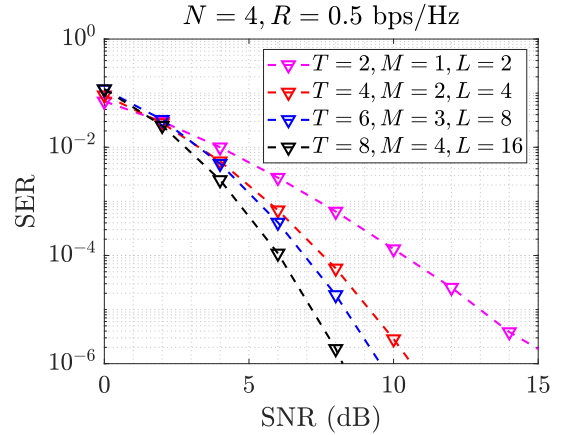


Fig. 3. SER results across different values of T and M for fixed values of receive antennas and spectral efficiency.

of Grassmannian signaling with values of N close to T , even when $T < M + N$.

Fig. 3 compares different values of T and M with fixed values of receive antennas, $N = 4$, and spectral efficiency, $R = 0.5$ bps/Hz. Remarkably, increasing the pair (T, M) consistently leads to improved SER performance, even though this implicitly requires increasing the number of constellation points L to maintain the spectral efficiency. This condition ensures that the designed algorithm effectively exploits an increment in the dimensionality of the Grassmann manifold.

Finally, Fig. 4 presents results for all possible values of L with $T = 4$, $M = 2$, and $N = 2$. For $L = 2$, $L = 4$, $L = 8$, and $L = 16$, Case (i), Case (ii), Case (iii), and Case (iv) are applied in Algorithm 1, respectively. Furthermore, for $L = 16$, a comparison is presented between using DP (the default choice) and UB for adjusting geodesic mapping (see Section IV-B). As predicted in Section IV-B, since the constellation points obtained in the Grassmann manifold using both strategies are very similar (Fig. 1b), their error performance is nearly identical. Note that, for $L = 4$ under Case (ii), the same constellation points are obtained, as shown in Fig. 1a.

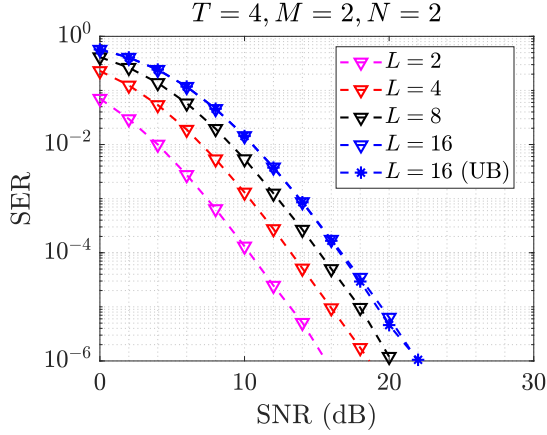


Fig. 4. SER results for all possible values of L and fixed values of T , M , and N . Considering UB instead of DP for geodesic mapping in Algorithm 1 is denoted as (UB).

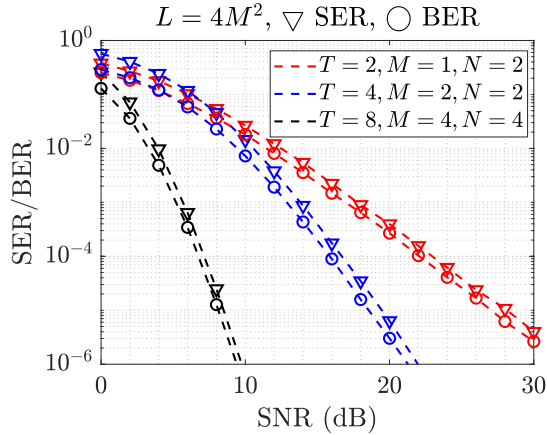


Fig. 5. Evaluation of bit labeling performance, comparing SER and BER results for equal values of T , M , N , and L .

B. BER versus SER

In Fig. 5, the bit labeling strategy described in Section IV-C is evaluated by comparing SER and BER results across different values of T , M , N , and L , always using the maximum possible values of L , which for the considered cases are $L = 4$, $L = 16$, and $L = 64$ for $M = 1$, $M = 2$, and $M = 4$, respectively. For $M = 2$ and $M = 4$, the relation $\text{BER} \approx \frac{1}{2}\text{SER}$ is observed, which corresponds to the expected BER under the assumption that codewords with maximum Hamming distance have a negligible PEP, while all other codewords are equally likely to be mistaken. This validates the design goal of avoiding errors between codewords with maximum Hamming distance. For $M = 1$, we obtain $\text{BER} \approx \frac{2}{3}\text{SER}$, since in this particular case with $L = 4$, the DP (as well as the chordal and geodesic distances) are nearly identical across all codeword pairs.

C. Comparison with Other Approaches

Finally, we compare the SER performance of our proposed design with other algorithms from the literature. In particular, Fig. 4 shows the SER results for the maximum number of points $L = 4M^2$ allowed by our design (Geod.), compared

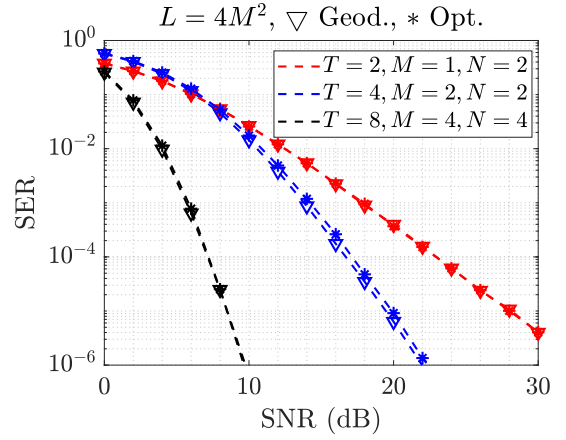


Fig. 6. SER comparison between the proposed Grassmannian constellation design (Geod.) and the DP gradient optimization presented in [26] (Opt.).

with the DP gradient ascent optimization proposed in [26] (Opt.), for which the code is publicly available [5]. Table IV reports the corresponding values of the DP and chordal distance for the constellations obtained with both strategies. For $(T, M) = (2, 1)$ with $L = 4$, the performance is identical in both cases. For $(T, M) = (4, 2)$ with $L = 16$, the geodesic mapping approach improves upon the optimization in terms of DP, resulting in slightly better SER performance. Remarkably, for $(T, M) = (8, 4)$ with $L = 64$, Case (v) of Algorithm 1 is applied. In this case, the proposed design does not use DP as the objective function but instead relies on the chordal distance, as explained in Section IV-B. As a result, the obtained DP is 0, while the chordal distance is excellent, with a minimum value of $\sqrt{M}/\sqrt{2}$ when mapping all geodesics ($L = 64$), where the maximum possible chordal distance between two points is $\sqrt{M} = 2$. Notably, SER results in this case are nearly identical to those obtained with DP optimization. This is because, for the considered values $T = 2M$ with $M = N = 4$, the SER values of interest lie in the low-SNR range (below 10 dB), where the chordal distance serves as a reliable predictor of the PEP (Section III).

In [5, Fig. 3.4], it can be observed that, using the UB optimization proposed in [18] with $T = 4$, $M = 2$, $N = 2$, $L = 16$, and $\text{SNR} = 20$ dB, the obtained SER is about 10^{-5} , similar to that achieved with the DP optimization in Fig. 6, and slightly worse than our result. In general, results obtained with UB optimization have been shown to slightly improve upon those of DP optimization [5, Fig. 3.5], and thus, we expect them to be comparable to the results achieved with our approach. Note that the main advantage of the UB optimization presented in [18] is its applicability to arbitrary values of T , M , N , and L , whereas our design is constrained in spectral efficiency by the condition $2 \leq L \leq 4M^2$. On the other hand, for the considered values of L , the geodesic mapping approach has the important advantage of requiring only one active antenna per time slot, without degrading SER performance compared to state-of-the-art unstructured Grassmannian constellation designs.

For additional reference, in Fig. 7 we compare the obtained BER results for the proposed noncoherent design with those of

TABLE IV

COMPARISON OF DP AND CHORDAL DISTANCE BETWEEN THE PROPOSED ALGORITHM AND THE OPTIMIZATION PRESENTED IN [26] FOR $L = 4M^2$.

(T, M)	Proposed		Optimization [26]	
	$DP(\mathcal{X})$	$d_c(\mathcal{X})$	$DP(\mathcal{X})$	$d_c(\mathcal{X})$
(2, 1)	0.6665	0.8164	0.6665	0.8164
(4, 2)	0.1715	0.9102	0.1263	0.8494
(8, 4)	0	1.4142	0.0046	1.1467

space-time block coding (STBC) strategies that assume perfect CSIR but no CSIT [37]. For $M = N = 2$, the noncoherent design (Noncoh.) uses the maximum spectral efficiency with $T = 4$ and $L = 16$ points, yielding $R = 1$ bps/Hz. For a fair comparison, the same spectral efficiency is selected for the STBC design (noted as CSIR), which in this case is based on the well-known Alamouti scheme with two transmit antennas [38]. Although this design strictly requires only a time block of $T = 2$ if CSIR is already available, under the assumption of a block-fading channel with $T = 4$, reliable CSIR acquisition within each block requires the transmitter to allocate M time slots for transmitting orthogonal pilot symbols from each antenna [2]. As a result, within $T = 4$ time slots, only two information symbols are transmitted, requiring the use of a QPSK constellation (instead of BPSK) to achieve $R = 1$ bps/Hz, assuming that pilot symbols have the same average power as information symbols. Under these conditions, perfect CSIR is assumed in Monte Carlo simulations, and the Alamouti scheme shows a consistent improvement in SER performance compared to the noncoherent approach, with an observed gap of about 2 dB at high SNR. However, note that the Alamouti scheme, applicable only to $M = 2$, offers the best performance among STBC designs that rely on CSIR, due to its ability to simultaneously achieve full rate, full diversity, and symbol orthogonality, which is not possible for $M > 2$ [37]. For $M = N = 4$, the noncoherent strategy uses $L = 64$ with $T = 8$, yielding $R = 0.75$ bps/Hz. To preserve full diversity and symbol orthogonality, the STBC design adopts a 3/4 rate scheme, meaning that only three information symbols are transmitted over every four time slots [37], [39]. The same conditions for acquiring CSIR apply, resulting in a QPSK constellation achieving a rate of 0.75 bps/Hz. In this case, it can be observed that the noncoherent strategy outperforms the coherent approach as the SNR increases. Finally, it should be noted that CSIR, while more feasible to obtain than CSIT, would never be perfect in a practical implementation due to at least the impact of AWGN during pilot transmission and reception. Additionally, its use inevitably increases system complexity at both the transmitter and the receiver, and, even for $M = 2$, implementing Alamouti coding requires more than one active antenna per time slot in transmission.

VI. CONCLUSION

In this work, a structured family of Grassmannian constellations for MIMO noncoherent communications is presented. We begin by reviewing the system model and the

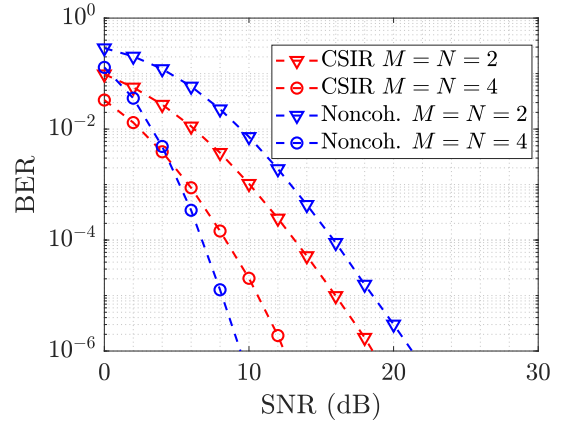


Fig. 7. SER comparison for equal spectral efficiency between the proposed noncoherent design and STBC strategies relying on CSIR. Spectral efficiencies are 1 and 0.75 bps/Hz for $M = N = 2$ and $M = N = 4$, respectively.

metrics associated with the Grassmann manifold that have been previously analyzed in relation to SEP and PEP. Then, we present the proposed algorithm, which is based on computing and mapping geodesic curves on the Grassmann manifold departing from an initial point with a suitable set of initial velocities or vectors. These initial velocities are systematically constructed using the canonical matrix representation of the finite-dimensional Weyl–Heisenberg group, although other sets of vectors satisfying the required properties could also be used. In this manner, we obtain the property that all points or matrices in the unitary space-time constellation contain a single nonzero entry per row, meaning that only one transmit antenna is active per time slot. This feature reduces hardware complexity, implementation cost, and power consumption, since only one DAC and one power amplifier are required for transmission, and decreases the computational cost of ML detection by a factor of M . Considering $T = 2M$, and taking at most one point per computed geodesic (except for $L = 2$), the design limits the maximum number of points to twice the dimension of the complex Grassmannian (as a real manifold), i.e., $L \leq 4M(2M - M) = 4M^2$. Although this restricts spectral efficiency to the range of 0.25–1 bps/Hz for the combinations of T and L of interest, this range is well suited to many use cases where noncoherent communications are applicable, such as short-packet URLLC communications in mobile scenarios where CSI acquisition is costly or unreliable. Furthermore, this design may be applicable to scenarios where SIMO has previously been considered, such as the uplink in IoT networks, by simply adding more antennas and a switching mechanism to the single-antenna transmitter.

Within the considered number of points L , the geodesic mapping can be adjusted to achieve good performance in terms of metrics related to SEP and PEP, while also allowing for a simple bit-labeling strategy that minimizes PEP between codewords with maximum Hamming distance. All of these properties are validated through Monte Carlo simulations for SER and BER. Remarkably, the proposed constellations achieve SER performance comparable to state-of-the-art unstructured designs, while maintaining their unique structure.

While it is not always possible to achieve a nonzero DP (also known as a full diversity constellation or code), two factors mitigate its impact on error performance. First, in those cases, excellent chordal distance is achieved instead. Second, this situation arises only for $M \geq 3$, where, considering $N \geq M$, and given the relatively low number of points L , the SER values of interest fall within the low-SNR range, in which chordal distance serves as a good metric for reducing PEP. Finally, for additional reference, a comparison is presented with standard coherent STBC schemes that rely solely on CSIR. Even assuming perfect CSIR, Grassmannian signaling outperforms the coherent approach when the Alamouti code cannot be applied for $M > 2$, and the considered STBC designs require more than one active antenna per time slot.

Examples of constellations obtained with our design can be found at: <https://github.com/alvpr/grassmannian>.

APPENDIX

A. Theoretical Background

In this section, we present the background that provides the theoretical foundation of the paper, focusing on the elements that are explicitly used in this work. All of this material is standard and can be found, for example, in [11] and [40].

The *complex Grassmann manifold* or *complex Grassmannian* $\text{Gr}_{\mathbb{C}}(T, M)$ is defined as the set of all M -dimensional complex subspaces \mathcal{U} of \mathbb{C}^T . Each such subspace \mathcal{U} can be represented by a matrix $\mathbf{U} \in \mathbb{C}^{T \times M}$ whose M column vectors form an orthonormal basis of \mathcal{U} ; we write in this case $\mathcal{U} = \text{span}(\mathbf{U})$. These matrices are elements of the *complex Stiefel manifold*

$$\text{St}_{\mathbb{C}}(T, M) := \{\mathbf{U} \in \mathbb{C}^{T \times M} : \mathbf{U}^H \mathbf{U} = \mathbf{I}_M\}.$$

Given \mathcal{U} , there is a unique orthogonal projector \mathbf{P} onto \mathcal{U} , that is, there exists a unique matrix $\mathbf{P} \in \mathbb{C}^{T \times T}$ such that $\mathbf{P}^H = \mathbf{P}$, $\mathbf{P}^2 = \mathbf{P}$, and $\text{range}(\mathbf{P}) = \mathcal{U}$, which is given by $\mathbf{P} = \mathbf{U} \mathbf{U}^H$ for any $\mathbf{U} \in \text{St}_{\mathbb{C}}(T, M)$ such that $\mathcal{U} = \text{span}(\mathbf{U})$. Therefore, for any two matrices $\mathbf{U}_1, \mathbf{U}_2 \in \text{St}_{\mathbb{C}}(T, M)$, it holds that $\text{span}(\mathbf{U}_1) = \text{span}(\mathbf{U}_2)$ if and only if $\mathbf{U}_2 \mathbf{U}_2^H = \mathbf{U}_1 \mathbf{U}_1^H$ or, equivalently, if and only if $\mathbf{U}_2 = \mathbf{U}_1 \mathbf{R}$, where $\mathbf{R} \in \mathbb{C}^{M \times M}$ is an element of the *unitary group*

$$U(M) := \{\mathbf{R} \in \mathbb{C}^{M \times M} : \mathbf{R}^H \mathbf{R} = \mathbf{I}_M = \mathbf{R} \mathbf{R}^H\}.$$

This means that $\text{Gr}_{\mathbb{C}}(T, M)$ can be identified with the quotient space $\text{St}_{\mathbb{C}}(T, M)/U(M)$, i.e., each element $\mathcal{U} = \text{span}(\mathbf{U})$ of $\text{Gr}_{\mathbb{C}}(T, M)$ uniquely corresponds to the *equivalence class*

$$[\mathbf{U}] := \{\mathbf{U}_1 \in \text{St}_{\mathbb{C}}(T, M) : \mathbf{U}_1 = \mathbf{U} \mathbf{R}, \mathbf{R} \in U(M)\},$$

which, in turn, uniquely corresponds to the orthogonal projector $\mathbf{P}_{[\mathbf{U}]} := \mathbf{U} \mathbf{U}^H$ onto \mathcal{U} . We say that $\mathbf{U} \in \text{St}_{\mathbb{C}}(T, M)$ is a *Stiefel representative* of the subspace $\mathcal{U} = \text{span}(\mathbf{U})$. Throughout this work, we identify $\mathcal{U} \equiv [\mathbf{U}]$ and write the elements of the Grassmannian as $[\mathbf{U}] \in \text{Gr}_{\mathbb{C}}(T, M)$.

$\text{Gr}_{\mathbb{C}}(T, M) = \text{St}_{\mathbb{C}}(T, M)/U(M)$ can be endowed with a differential structure that makes it a real compact manifold of dimension $2M(T - M)$. At each $[\mathbf{U}] \in \text{Gr}_{\mathbb{C}}(T, M)$, the tangent space can be identified with

$$T_{[\mathbf{U}]} \text{Gr}_{\mathbb{C}}(T, M) = \{\Delta \in \mathbb{C}^{T \times M} : \mathbf{U}^H \Delta = 0\}. \quad (11)$$

We also endow $\text{Gr}_{\mathbb{C}}(T, M)$ with the following Riemannian metric:

$$g_{[\mathbf{U}]}(\Delta_1, \Delta_2) := \Re \operatorname{tr}(\Delta_1^H \Delta_2), \quad (12)$$

and given any curve $\gamma : [t_1, t_2] \rightarrow \text{Gr}_{\mathbb{C}}(T, M)$, we define its *g-length* as

$$L_g(\gamma) := \int_{t_1}^{t_2} \sqrt{g_{\gamma(t)}(\dot{\gamma}(t), \dot{\gamma}(t))} dt = \int_{t_1}^{t_2} \|\dot{\gamma}(t)\|_g dt,$$

where $\|\cdot\|_g := \sqrt{g(\cdot, \cdot)}$ is the *g-norm* and $\dot{\gamma}(t)$ denotes the velocity vector of the curve.

With this Riemannian metric, $\text{Gr}_{\mathbb{C}}(T, M)$ is actually a totally geodesic Riemannian submanifold of the *real Grassmann manifold* $\text{Gr}_{\mathbb{R}}(2T, 2M)$ of $2M$ -dimensional real subspaces of \mathbb{R}^{2T} , endowed with one half times the Frobenius (or Euclidean) metric, as in [11, Section 3.1]. This implies that all the formulas for angles, distances, and geodesics of the real Grassmannian translate exactly the same to the complex case, simply by replacing the transpose with the conjugate transpose. In particular:

- The *principal angles* $\theta_1, \dots, \theta_M \in [0, \frac{\pi}{2}]$ between two points $[\mathbf{U}_1], [\mathbf{U}_2] \in \text{Gr}_{\mathbb{C}}(T, M)$ are a measure of the “relative position” between the two complex subspaces $\mathcal{U}_1 = \text{span}(\mathbf{U}_1)$ and $\mathcal{U}_2 = \text{span}(\mathbf{U}_2)$. They can be computed as

$$\theta_m = \arccos(\sigma_m) \in \left[0, \frac{\pi}{2}\right], \quad m = 1, \dots, M, \quad (13)$$

where $\sigma_m \in [0, 1]$ is the m -th largest singular value of $\mathbf{U}_1^H \mathbf{U}_2$. This is independent of the chosen Stiefel representatives $\mathbf{U}_1, \mathbf{U}_2 \in \text{St}_{\mathbb{C}}(T, M)$. In this work we are most interested in the case where all the principal angles are nonzero, which means that $\mathcal{U}_1 \cap \mathcal{U}_2 = \{0\}$. If one principal angle is 0, then \mathcal{U}_1 and \mathcal{U}_2 share a nontrivial direction. If $\theta_m = 0$ for all m , then $\mathcal{U}_1 = \mathcal{U}_2$. In contrast, if one principal angle is $\frac{\pi}{2}$, there is a direction in \mathcal{U}_1 orthogonal to \mathcal{U}_2 , and vice versa. If $\theta_m = \frac{\pi}{2}$ for all m , then \mathcal{U}_1 and \mathcal{U}_2 are mutually orthogonal: every direction in \mathcal{U}_1 is orthogonal to every direction in \mathcal{U}_2 .

- The *Riemannian distance* d_g (induced by g in Eq. (12)) between two points $[\mathbf{U}_1], [\mathbf{U}_2] \in \text{Gr}_{\mathbb{C}}(T, M)$ can be computed as

$$d_g([\mathbf{U}_1], [\mathbf{U}_2]) = \left(\sum_{m=1}^M \theta_m^2 \right)^{1/2}, \quad (14)$$

where $\{\theta_m\}_{m=1}^M$ are the principal angles between both points. This directly implies that d_g is bounded by

$$d_g([\mathbf{U}_1], [\mathbf{U}_2]) \leq \sqrt{M} \frac{\pi}{2}, \quad \forall [\mathbf{U}_1], [\mathbf{U}_2] \in \text{Gr}_{\mathbb{C}}(T, M). \quad (15)$$

- Given a point $[\mathbf{U}] \in \text{Gr}_{\mathbb{C}}(T, M)$ and a vector $\Delta \in T_{[\mathbf{U}]} \text{Gr}_{\mathbb{C}}(T, M)$, the *geodesic* $\gamma_{\Delta}(t)$ (with respect to the Riemannian metric g in Eq. (12)) departing at $\gamma_{\Delta}(0) = [\mathbf{U}]$ with velocity $\dot{\gamma}_{\Delta}(0) = \Delta$ is given for any $t \in \mathbb{R}$ by

$$\gamma_{\Delta}(t) = [\mathbf{U} \mathbf{V} \cos(t\boldsymbol{\Sigma}) \mathbf{V}^H + \mathbf{Q} \sin(t\boldsymbol{\Sigma}) \mathbf{V}^H], \quad (16)$$

where the cosine and sine functions only apply to the diagonal entries of $t\boldsymbol{\Sigma}$, and $\Delta = \mathbf{Q} \boldsymbol{\Sigma} \mathbf{V}^H$ is the compact

singular value decomposition (SVD) of Δ , with $\mathbf{Q} \in \text{St}_{\mathbb{C}}(T, M)$, $\Sigma = \text{diag}(\sigma_1, \dots, \sigma_M)$, and $\mathbf{V} \in U(M)$.

Given two points $[\mathbf{U}_1], [\mathbf{U}_2] \in \text{Gr}_{\mathbb{C}}(T, M)$, there always exists a geodesic from $[\mathbf{U}_1]$ to $[\mathbf{U}_2]$ whose g -length is exactly $d_g([\mathbf{U}_1], [\mathbf{U}_2])$. This is why d_g in Eq. (14) is also called *geodesic distance*. Moreover, if we denote by $\gamma_{\Delta}|_{[t_1, t_2]}$ the restriction of the geodesic γ_{Δ} to the interval $[t_1, t_2]$, then the following equivalent properties hold for $t_2 - t_1 > 0$ small enough:

- (i) $\gamma_{\Delta}|_{[t_1, t_2]}$ locally realizes the Riemannian distance: the g -length of the geodesic segment $\gamma_{\Delta}|_{[t_1, t_2]}$ is exactly $d_g(\gamma_{\Delta}(t_1), \gamma_{\Delta}(t_2))$.
- (ii) $\gamma_{\Delta}|_{[t_1, t_2]}$ is locally minimizing: the g -length of any curve from $\gamma_{\Delta}(t_1)$ to $\gamma_{\Delta}(t_2)$ is greater than or equal to the g -length of $\gamma_{\Delta}|_{[t_1, t_2]}$.

However, these properties do not hold globally in general (for arbitrarily big $t_2 - t_1$). Given $[\mathbf{U}] \in \text{Gr}_{\mathbb{C}}(T, M)$, we define the *cut instant* of $\Delta \in T_{[\mathbf{U}]} \text{Gr}_{\mathbb{C}}(T, M)$ as

$$\text{Cut}_{[\mathbf{U}]}(\Delta) := \sup \{t > 0 : \gamma_{\Delta}|_{[0, t]} \text{ is minimizing}\},$$

which can be computed as

$$\text{Cut}_{[\mathbf{U}]}(\Delta) = \frac{\pi}{2\sigma_1}, \quad (17)$$

where σ_1 is the largest singular value of Δ .

When Δ is g -unit, i.e., $\|\Delta\|_g := \sqrt{g_{[\mathbf{U}]}(\Delta, \Delta)} = 1$, then the g -length of $\gamma_{\Delta}|_{[t_1, t_2]}$ is exactly $t_2 - t_1$, for all $t_2 > t_1$, and due to Eq. (15), the cut instant is bounded by

$$\text{Cut}_{[\mathbf{U}]}(\Delta) \leq \sqrt{M} \frac{\pi}{2}, \quad \forall g\text{-unit } \Delta \in T_{[\mathbf{U}]} \text{Gr}_{\mathbb{C}}(T, M).$$

We say that a g -unit vector Δ is a *diametral vector* if $\text{Cut}_{[\mathbf{U}]}(\Delta) = \sqrt{M} \frac{\pi}{2}$. This means that the geodesic γ_{Δ} travels the maximum possible distance in the manifold before properties (i) and (ii) cease to hold.

B. Proof of Theorem 1

If $\Delta \in T_{[\mathbf{U}]} \text{Gr}_{\mathbb{C}}(2M, M)$ is in the form of Eq. (8), with $\sqrt{M} \tilde{\Delta} \in U(M)$, then its SVD $\Delta = \mathbf{Q} \Sigma \mathbf{V}^H$ is given by

$$\mathbf{Q} = \begin{pmatrix} \mathbf{0}_M \\ \sqrt{M} \tilde{\Delta} \end{pmatrix}, \quad \Sigma = \frac{1}{\sqrt{M}} \mathbf{I}_M, \quad \mathbf{V} = \mathbf{I}_M,$$

and then, it is a straightforward computation to derive Eq. (9) from the geodesic expression in Eq. (16). Moreover, since $\Delta^H \Delta = \tilde{\Delta}^H \tilde{\Delta} = \frac{1}{M} \mathbf{I}_M$, clearly Δ is g -unit with all its singular values equal to $\frac{1}{\sqrt{M}}$. From Eq. (17), we obtain

$$\text{Cut}_{[\mathbf{U}]}(\Delta) = \sqrt{M} \frac{\pi}{2},$$

which means that Δ is a diametral vector.

C. Proof of Theorem 2

Let $\gamma_{\Delta_1}(t_1)$ and $\gamma_{\Delta_2}(t_2)$ be two geodesic points satisfying Eq. (9), with $t_1, t_2 \in (0, \sqrt{M} \frac{\pi}{2})$. This means that γ_{Δ_1} and γ_{Δ_2} depart from the same point $[\mathbf{U}]$ with initial velocities Δ_1 and Δ_2 , respectively, such that $\mathbf{W}_1 := \sqrt{M} \tilde{\Delta}_1$, $\mathbf{W}_2 :=$

$\sqrt{M} \tilde{\Delta}_2 \in U(M)$. By a slight abuse of notation, we identify each geodesic point with the Stiefel representative given by Eq. (9) and write

$$\Gamma(t_1, t_2) := \gamma_{\Delta_1}(t_1)^H \gamma_{\Delta_2}(t_2).$$

Then, using $\tilde{\mathbf{U}}^H \tilde{\mathbf{U}} = \mathbf{U}^H \mathbf{U} = \mathbf{I}_M$, a straightforward computation shows that

$$\Gamma(t_1, t_2) = \cos \alpha_1 \cos \alpha_2 \mathbf{I}_M + \sin \alpha_1 \sin \alpha_2 \mathbf{W}_1^H \mathbf{W}_2,$$

where $\alpha_1 := \frac{t_1}{\sqrt{M}}$ and $\alpha_2 := \frac{t_2}{\sqrt{M}}$. Therefore, $\Gamma(t_1, t_2)$ is a linear combination of \mathbf{I}_M and $\mathbf{W}_1^H \mathbf{W}_2$. This means, on the one hand, that $\Gamma(t_1, t_2)$ commutes with $\mathbf{W}_1^H \mathbf{W}_2$, so both matrices are simultaneously diagonalizable, i.e., the eigenvalues μ_m of $\Gamma(t_1, t_2)$ are given by

$$\mu_m = \cos \alpha_1 \cos \alpha_2 + \sin \alpha_1 \sin \alpha_2 \lambda_m, \quad m = 1, \dots, M, \quad (18)$$

where λ_m are the eigenvalues of $\mathbf{W}_1^H \mathbf{W}_2$. On the other hand, since \mathbf{I}_M and $\mathbf{W}_1^H \mathbf{W}_2$ are two commuting normal matrices (observe that $\mathbf{W}_1^H \mathbf{W}_2 \in U(M)$), then $\Gamma(t_1, t_2)$ is also normal, meaning that its singular values σ_m are given by

$$\sigma_m = |\mu_m|, \quad m = 1, \dots, M, \quad (19)$$

where $|\cdot|$ denotes the complex absolute value. Now, using that $\mathbf{W}_1^H \mathbf{W}_2$ is unitary, we can write its eigenvalues as $\lambda_m = e^{i\phi_m} = \cos \phi_m + i \sin \phi_m$, where i is the imaginary unit and $\phi_m \in [0, 2\pi)$. Then, from Eq. (18) we obtain:

$$\begin{aligned} |\mu_m|^2 &= (\cos \alpha_1 \cos \alpha_2 + \sin \alpha_1 \sin \alpha_2 \cos \phi_m)^2 \\ &\quad + (\sin \alpha_1 \sin \alpha_2 \sin \phi_m)^2. \end{aligned} \quad (20)$$

Consequently, for each eigenvalue λ_m of $\mathbf{W}_1^H \mathbf{W}_2 = M \tilde{\Delta}_1^H \tilde{\Delta}_2 = M \Delta_1^H \Delta_2$:

- If $\lambda_m = 1$, then $\phi_m = 0$ and

$$\sigma_m = |\cos \alpha_1 \cos \alpha_2 + \sin \alpha_1 \sin \alpha_2| = |\cos(\alpha_1 - \alpha_2)|.$$

- If $\lambda_m \neq 1$, then $\phi_m \neq 0$ (so $\cos \phi_m < 1$) and

$$\begin{aligned} \sigma_m &\leq |\cos \alpha_1 \cos \alpha_2 + \sin \alpha_1 \sin \alpha_2 \cos \phi_m| \\ &< |\cos(\alpha_1 - \alpha_2)| \leq 1. \end{aligned}$$

Finally, recall that the principal angles θ_m between $\gamma_{\Delta_1}(t_1)$ and $\gamma_{\Delta_2}(t_2)$ are given by $\theta_m = \arccos(\sigma_m)$ (see Eq. (13)), which means that $\theta_m = 0$ if and only if $\sigma_m = 1$. Taking all this into account, we conclude:

- If $t_1 \neq t_2$, then $\alpha_1 \neq \alpha_2$ and $\sigma_m < 1$ for all $m = 1, \dots, M$, i.e., all the principal angles θ_m are nonzero.
- If $t_1 = t_2$, then $\sigma_m = 1$ if and only if $\lambda_m = 1$, i.e., the number of principal angles θ_m equal to zero coincides with the number of eigenvalues λ_m equal to 1.

D. Proof of Corollary 1

Following the same notation as in the proof of Theorem 2 (Appendix-C) with $\Delta_1 = \Delta$ and $\Delta_2 = -\Delta$, note that all the eigenvalues $\lambda_m = e^{i\phi_m}$ of $-M \Delta^H \Delta = -\mathbf{I}_M$ are equal to -1 , i.e., $\phi_m = \pi$ for all $m = 1, \dots, M$. Using Eq. (19) and

Eq. (20) with $\phi_m = \pi$ and $t_1 = t_2 = \sqrt{M}\frac{\pi}{4}$ ($\alpha_1 = \alpha_2 = \frac{\pi}{4}$), we obtain:

$$\begin{aligned}\sigma_m &= |\cos \alpha_1 \cos \alpha_2 - \sin \alpha_1 \sin \alpha_2| = |\cos(\alpha_1 + \alpha_2)| \\ &= \cos\left(\frac{\pi}{2}\right) = 0, \quad m = 1, \dots, M,\end{aligned}$$

which means that all the principal angles $\theta_m = \arccos(\sigma_m)$ between both geodesic points are equal to $\frac{\pi}{2}$.

REFERENCES

- [1] E. G. Larsson, O. Edfors, F. Tufvesson, and T. L. Marzetta, "Massive MIMO for Next Generation Wireless Systems," *IEEE Commun. Mag.*, vol. 52, pp. 186–195, Feb. 2014.
- [2] B. Hassibi and B. Hochwald, "How Much Training is Needed in Multiple-Antenna Wireless Links?," *IEEE Trans. Inf. Theory*, vol. 49, pp. 951–963, Apr. 2003.
- [3] B. Clerckx, H. Joudah, C. Hao, M. Dai, and B. Rassouli, "Rate Splitting for MIMO Wireless Networks: a Promising PHY-Layer Strategy for LTE evolution," *IEEE Commun. Mag.*, vol. 54, pp. 98–105, May 2016.
- [4] Á. Pendás-Recondo, J. A. López-Fernández, and R. G. Ayestarán, "On the MISO Broadcast Channel With Finite Constellations and Imperfect CSIT: Rate-Splitting, SDMA, NOMA, and Space-Time Block Coding," *IEEE OJ-COMS*, pp. 1–1, 2025.
- [5] D. Cuevas, *Advanced Grassmannian Constellation Designs for Noncoherent MIMO Communications*. PhD thesis, Universidad de Cantabria, Spain, Nov. 2024. Software available at <https://github.com/diegocuevasfdez/grassbox/>.
- [6] T. Marzetta and B. Hochwald, "Capacity of a Mobile Multiple-Antenna Communication Link in Rayleigh Flat Fading," *IEEE Trans. Inf. Theory*, vol. 45, pp. 139–157, Jan. 1999.
- [7] B. Hochwald and T. Marzetta, "Unitary Space-Time Modulation for Multiple-Antenna Communications in Rayleigh Flat Fading," *IEEE Trans. Inf. Theory*, vol. 46, pp. 543–564, Mar. 2000.
- [8] M. Brehler and M. Varanasi, "Asymptotic Error Probability Analysis of Quadratic Receivers in Rayleigh-fading Channels with Applications to a Unified Analysis of Coherent and Noncoherent Space-Time Receivers," *IEEE Trans. Inf. Theory*, vol. 47, pp. 2383–2399, Sept. 2001.
- [9] L. Zheng and D. Tse, "Communication on the Grassmann Manifold: a Geometric Approach to the Noncoherent Multiple-Antenna Channel," *IEEE Trans. Inf. Theory*, vol. 48, pp. 359–383, Feb. 2002.
- [10] B. Hassibi and T. Marzetta, "Multiple-Antennas and Isotropically Random Unitary Inputs: The Received Signal Density in Closed Form," *IEEE Trans. Inf. Theory*, vol. 48, pp. 1473–1484, June 2002.
- [11] T. Bendokat, R. Zimmermann, and P. Absil, "A Grassmann Manifold Handbook: Basic Geometry and Computational Aspects," *Adv. Comput. Math.*, vol. 50, no. 6, 2024.
- [12] J. H. Conway, R. H. Hardin, and N. J. A. Sloane, "Packing lines, planes, etc.: Packings in grassmannian spaces," *Experimental Mathematics*, vol. 5, no. 2, pp. 139–159, 1996.
- [13] R. H. Gohary and T. N. Davidson, "Noncoherent MIMO Communication: Grassmannian Constellations and Efficient Detection," *IEEE Trans. Inf. Theory*, vol. 55, pp. 1176–1205, Mar. 2009.
- [14] J. Álvarez Vizoso, D. Cuevas, C. Beltrán, I. Santamaría, V. Tuček, and G. Peters, "Constrained Riemannian Noncoherent Constellations for the MIMO Multiple Access Channel," *IEEE Trans. Inf. Theory*, vol. 69, pp. 4559–4578, July 2023.
- [15] M. Beko, J. Xavier, and V. A. N. Barroso, "Noncoherent Communication in Multiple-Antenna Systems: Receiver Design and Codebook Construction," *IEEE Trans. Signal Process.*, vol. 55, pp. 5703–5715, Dec. 2007.
- [16] G. Han and J. Rosenthal, "Geometrical and Numerical Design of Structured Unitary Space-Time Constellations," *IEEE Trans. Inf. Theory*, vol. 52, pp. 3722–3735, Aug. 2006.
- [17] M. McCloud, M. Brehler, and M. Varanasi, "Signal Design and Convolutional Coding for Noncoherent Space-Time Communication on the Block-Rayleigh-Fading Channel," *IEEE Trans. Inf. Theory*, vol. 48, pp. 1186–1194, May 2002.
- [18] D. Cuevas, J. Álvarez Vizoso, C. Beltrán, I. Santamaría, V. Tuček, and G. Peters, "Union Bound Minimization Approach for Designing Grassmannian Constellations," *IEEE Trans. Commun.*, vol. 71, pp. 1940–1952, Apr. 2023.
- [19] B. Hochwald, T. Marzetta, T. Richardson, W. Sweldens, and R. Urbanke, "Systematic Design of Unitary Space-time Constellations," *IEEE Trans. Inf. Theory*, vol. 46, pp. 1962–1973, Sep. 2000.
- [20] I. Kammoun and J.-C. Belfiore, "A New Family of Grassmann Space-Time Codes for Non-Coherent MIMO Systems," *IEEE Commun. Lett.*, vol. 7, no. 11, pp. 528–530, 2003.
- [21] I. Kammoun, A. M. Cipriano, and J.-C. Belfiore, "Non-Coherent Codes over the Grassmannian," *IEEE Trans. Wireless Commun.*, vol. 6, pp. 3657–3667, Oct. 2007.
- [22] G. Han and J. Rosenthal, "Geometrical and Numerical Design of Structured Unitary Space-Time Constellations," *IEEE Trans. Inf. Theory*, vol. 52, pp. 3722–3735, Aug. 2006.
- [23] D. Cuevas, C. Beltrán, M. Gutiérrez, I. Santamaría, and V. Tuček, "Structured Multi-Antenna Grassmannian Constellations for Noncoherent Communications," in *2024 IEEE 13rd Sensor Array and Multichannel Signal Processing Workshop (SAM)*, (Corvallis, OR, USA), pp. 1–5, 2024.
- [24] M. Beko, J. Xavier, and V. A. N. Barroso, "Noncoherent Communication in Multiple-Antenna Systems: Receiver Design and Codebook Construction," *IEEE Trans. Signal Process.*, vol. 55, pp. 5703–5715, Dec. 2007.
- [25] R. H. Gohary and T. N. Davidson, "Noncoherent MIMO Communication: Grassmannian Constellations and Efficient Detection," *IEEE Trans. Inf. Theory*, vol. 55, pp. 1176–1205, Mar. 2009.
- [26] J. Álvarez Vizoso, D. Cuevas, C. Beltrán, I. Santamaría, V. Tuček, and G. Peters, "Coherence-Based Subspace Packings for MIMO Noncoherent Communications," in *2022 30th European Signal Processing Conference (EUSIPCO)*, (Belgrade, Serbia), pp. 1906–1910, IEEE, 2022.
- [27] D. Cuevas, J. Álvarez Vizoso, C. Beltrán, I. Santamaría, V. Tuček, and G. Peters, "Constellations on the Sphere With Efficient Encoding-Decoding for Noncoherent Communications," *IEEE Trans. Wireless Commun.*, vol. 23, pp. 1886–1898, Mar. 2024.
- [28] S. T. Duong, H. H. Nguyen, E. Bedeer, and R. Barton, "Design and Detection of Unitary Constellations in Non-Coherent SIMO Systems for Short Packet Communications," *IEEE Trans. Wireless Commun.*, vol. 23, no. 10, pp. 12873–12887, 2024.
- [29] H. Meng, L. Zheng, C. Yang, J. Chen, X. Deng, and J. Wang, "Constellation Optimization and Energy Difference Detection in Massive SIMO Systems With Rician Channels," *IEEE Trans. Commun.*, vol. 73, pp. 6928–6942, Aug. 2025.
- [30] R. K. Mallik, "Multi-Level Signaling With Noncoherent SIMO Over a Rayleigh Channel," *IEEE Trans. Wireless Commun.*, vol. 23, pp. 16139–16154, Nov. 2024.
- [31] J. Álvarez Vizoso, D. Cuevas, C. Beltrán, I. Santamaría, V. Tuček, and G. Peters, "Constrained Riemannian Noncoherent Constellations for the MIMO Multiple Access Channel," *IEEE Trans. Inf. Theory*, vol. 69, pp. 4559–4578, July 2023.
- [32] S. Sanaye and A. Nosratinia, "Antenna Selection in MIMO Systems," *IEEE Commun. Mag.*, vol. 42, pp. 68–73, Oct. 2004.
- [33] W. Yang, G. Durisi, and E. Riegler, "On the Capacity of Large-MIMO Block-Fading Channels," *IEEE J. Sel. Areas Commun.*, vol. 31, pp. 117–132, Feb. 2013.
- [34] M. Brehler and M. Varanasi, "Asymptotic Error Probability Analysis of Quadratic Receivers in Rayleigh-Fading Channels with Applications to a Unified Analysis of Coherent and Noncoherent Space-Time Receivers," *IEEE Trans. Inf. Theory*, vol. 47, pp. 2383–2399, Sept. 2001.
- [35] I. Bengtsson and K. Życzkowski, *Geometry of Quantum States: An Introduction to Quantum Entanglement*. Cambridge University Press, 2 ed., 2017.
- [36] S. D. Howard, A. R. Calderbank, and W. Moran, "The Finite Heisenberg-Weyl Groups in Radar and Communications," *EURASIP J. Adv. Signal Process.*, no. 085685, 2006.
- [37] H. Jafarkhani, *Space-Time Coding: Theory and Practice*. USA: Cambridge University Press, 1st ed., 2010.
- [38] S. Alamouti, "A Simple Transmit Diversity Technique for Wireless Communications," *IEEE J. Sel. Areas Commun.*, vol. 16, pp. 1451–1458, Oct. 1998.
- [39] V. Tarokh, H. Jafarkhani, and A. Calderbank, "Space-Time Block Codes from Orthogonal Designs," *IEEE Trans. Inf. Theory*, vol. 45, pp. 1456–1467, July 1999.
- [40] A. Machado and I. M. C. Salavessa, "Grassmann Manifolds as Subsets of Euclidean Spaces," in *Differential Geometry (Santiago de Compostela, 1984)*, vol. 131 of *Research Notes in Mathematics*, pp. 85–102. Pitman, Boston, MA (1985).